Supporting Information

Accelerated HER kinetics via electron-deficient Ni and electron-enriched Se sites by dual Fe and Mn doping towards highly efficient hydrogen production

Guanglin Zhu[a], Lili Ren[c], Bo Gao[b], Cean Guo[a*], Jianjia Mu[d*], Fang Gu[e*], Zhongbao Feng[b*]

[a] *School of Equipment Engineering, Shenyang Ligong University, Shenyang 110159, China*

[b] *Key Laboratory for Ecological Metallurgy of Multimetallic Mineral (Ministry of Education), Northeastern University, Shenyang, 110819, China*

[c] *Shenyang Aircraft Industry (Group) Co. Ltd., Shenyang, 110034, China*

[d] *Dalian Institute of Chemical Physics, Chinese Academy of Sciences, Dalian, 116023, China*

[e] *College of Chemistry and Materials Science, Hebei University, Baoding, 071002, China*

[*] Corresponding authors. E-mail addresses: bigocean@163.com (C. Guo), mujianjia@dicp.ac.cn (J. Mu), fanggu@hbu.edu.cn, (F. Gu), fengzb@smm.neu.edu.cn (Z. Feng)

Experimental section

Chemicals

The following chemicals were used without further treatment: manganese chloride hexahydrate ($MnCl_2 \cdot 4H_2O$), nickel nitrate hexahydrate ($Ni(NO_3)_2 \cdot 6H_2O$), iron nitrate hexahydrate ($Fe(NO_3)_3 \cdot 9H_2O$), ammonium chloride (NH_4Cl), Se powder and potassium hydroxide (KOH) were purchased from Aladdin Reagents Ltd. The nickel foam (NF, 1.70 mm) was provided by Tianjin An Nuohe Chemical Industry-Trade Co., Ltd.

Electrochemical measurements

The HER performance of the catalysts was performed on CHI660e workstation with a three-electrode setup in 1.0 M KOH electrolyte. The as-prepared electrocatalysts were used as working electrodes, and Pt sheet and Hg/HgO were used as counter electrode and reference electrode, respectively. The HER activity of $Ni_{0.85}Se$, Fe-$Ni_{0.85}Se$ and Fe/Mn-$Ni_{0.85}Se$ was evaluated via polarization plots with 95% *IR* correction at a scan rate of 5 $mV \cdot s^{-1}$. The *R* was the solution resistance, which measured for all electrocatalysts based on electrochemical impedance spectroscopy (EIS). EIS was performed from 10^5 to10^{-2} Hz. The potentials were converted into reversible hydrogen electrode (RHE): $E_{RHE} = E_{SCE} + 0.059pH + 0.098$ without special illustration. Electrochemical surface area (ECSA) was measured by cyclic voltammetry (CV) with different scan rates to determine the double-layer capacitance (C_{dl}). The stability of the samples was determined by polarization plots after 5000 cycles, chronoamperometry and multi-current plot.

Theorical calculations

Theoretically calculations were performed with Vienna Ab Initio Simulation Package (VASP) according to density functional theory (DFT). Fe/Mn-$Ni_{0.85}Se$ was applied for the bulk structure. $Ni_{0.85}Se$ (101) was employed to generate the surface. Also, no strain and other external ambient pH and potentials were employed for the models during calculation. Electronic exchange-correction interaction was determined by GGA with Predew-Burke and Ernzerhof (PBE). The energy cutoff of 450 eV and iteration of 10^{-5} eV were adopted. A 15 Å vacuum was employed to separate the slab in z direction. A k-point mesh (3∗3∗1) was applied.

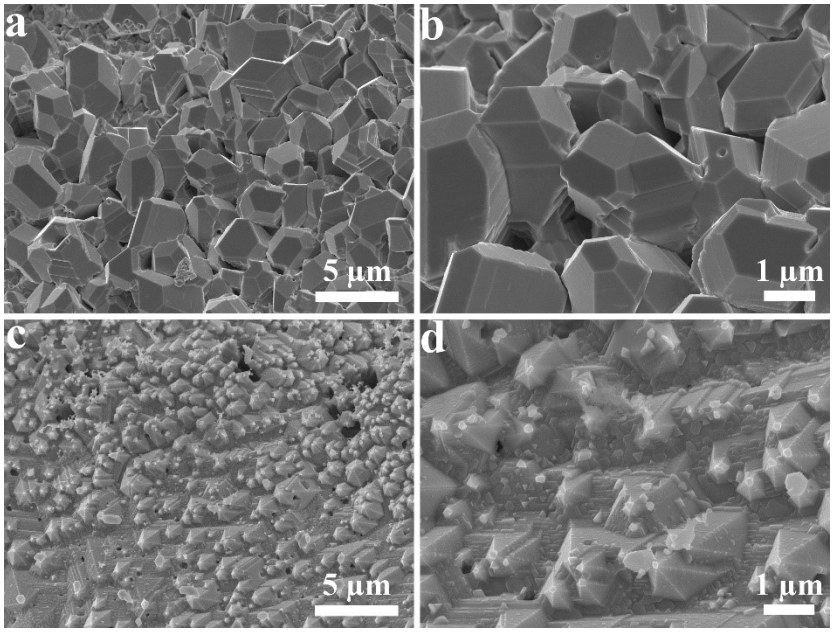

Figure S1 SEM images of (a,b) $Ni_{0.85}Se$ and (c,d) Fe-$Ni_{0.85}Se$.

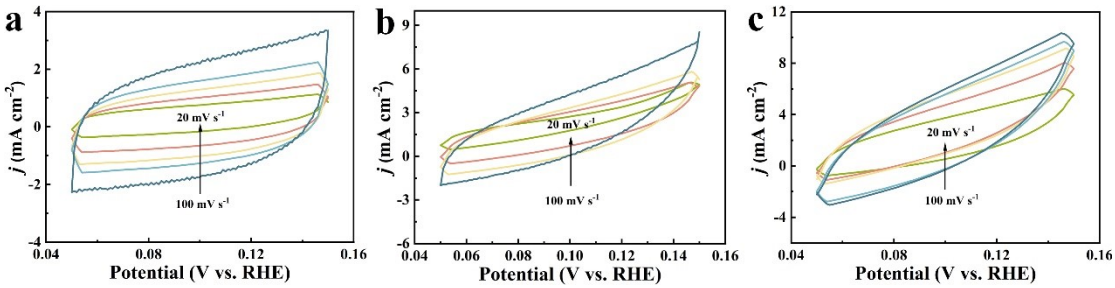

Figure S2 CV curves of (a) $Ni_{0.85}Se$, (b) Fe-$Ni_{0.85}Se$ and (c) Fe/Mn-$Ni_{0.85}Se$ in the capacitance current range at various scan rates.

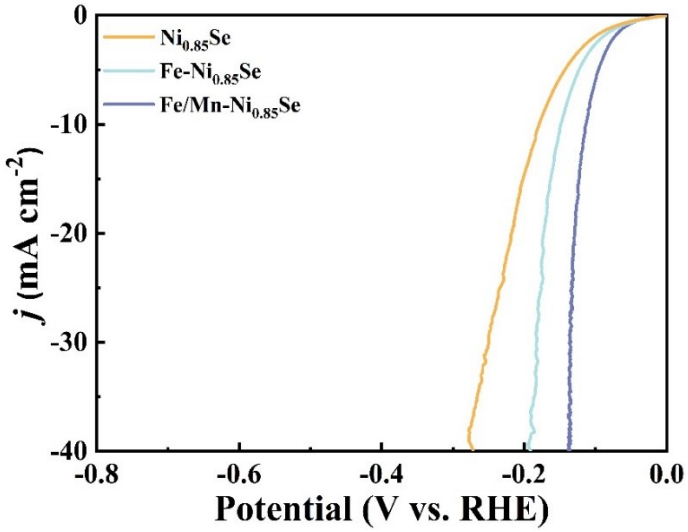

Figure S3 LSV plots of $Ni_{0.85}Se$, Fe-$Ni_{0.85}Se$ and Fe/Mn-$Ni_{0.85}Se$ after normalized by ECSA.

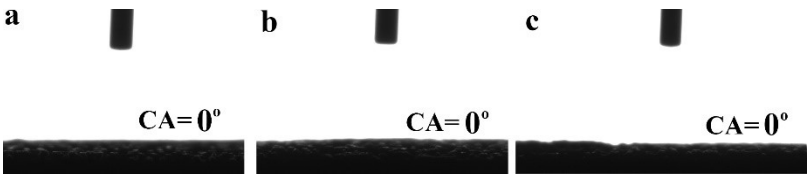

Figure S4 The contact angles of (a) $Ni_{0.85}Se$, (b) Fe-$Ni_{0.85}Se$ and (c) Fe/Mn-$Ni_{0.85}Se$.

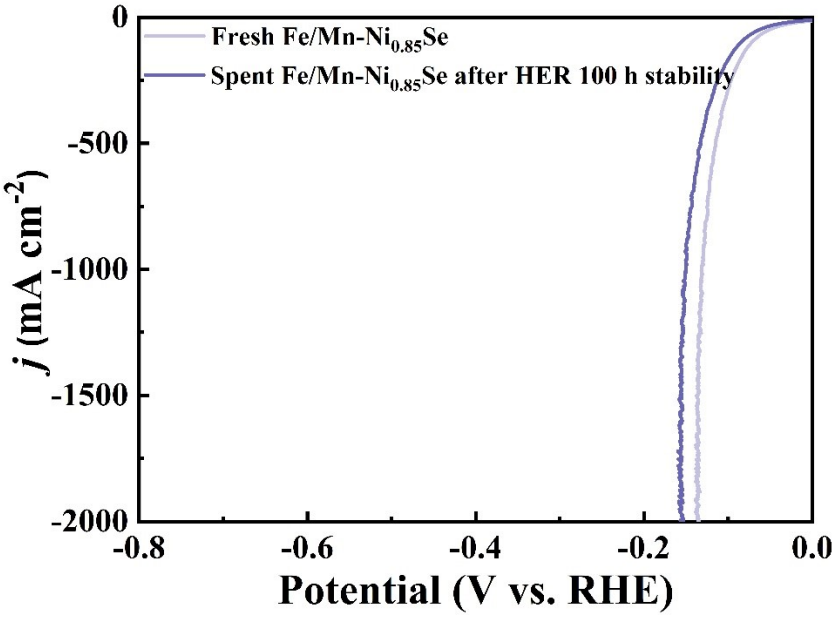

Figure S5 The polarization plots of Fe/Mn-$Ni_{0.85}Se$ before and after 100 h HER stability tests.

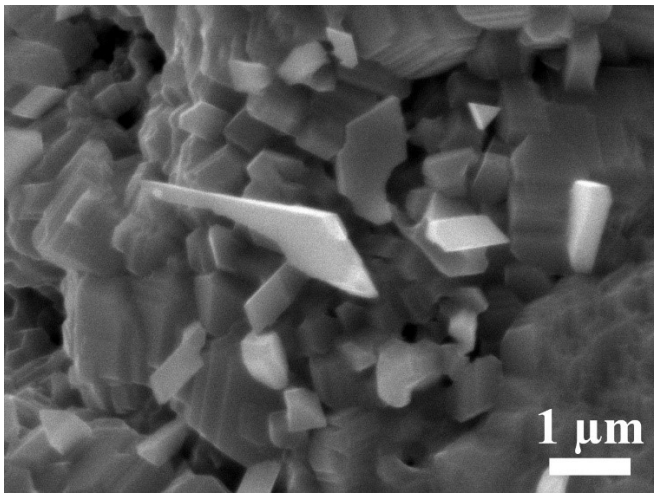

Figure S6 SEM images of Fe/Mn-$Ni_{0.85}Se$ after 100 h HER long-term stability test.

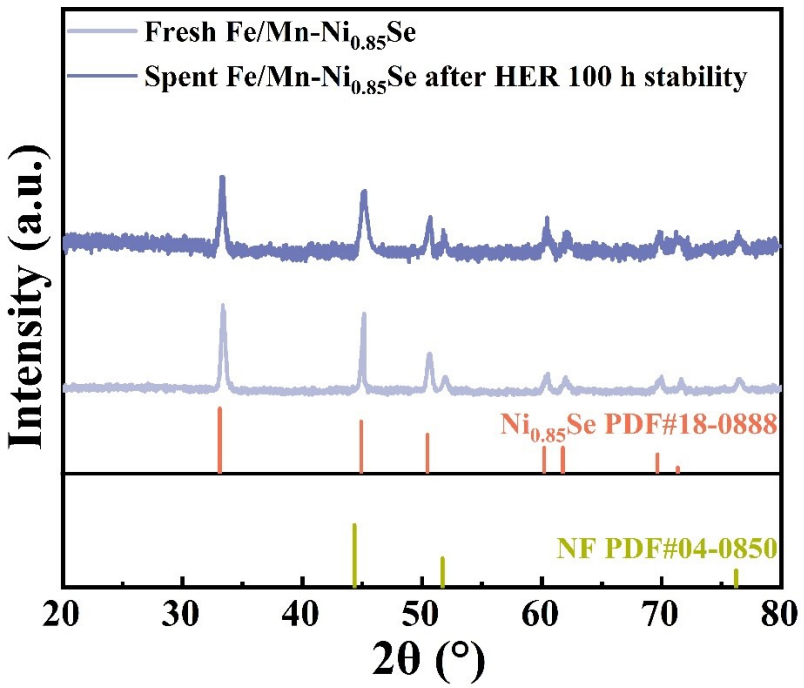

Figure S7 XRD patterns of Fe/Mn-$Ni_{0.85}Se$ before and after 100 h HER long-term stability tests.

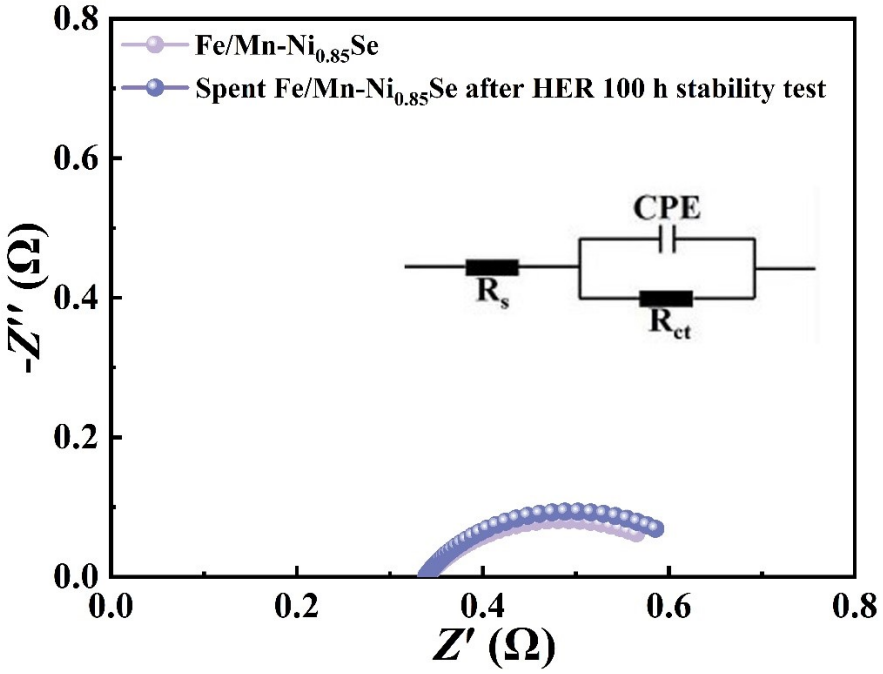

Figure S8 EIS plots of Fe/Mn-$Ni_{0.85}Se$ before and after 100 h HER long-term stability tests.

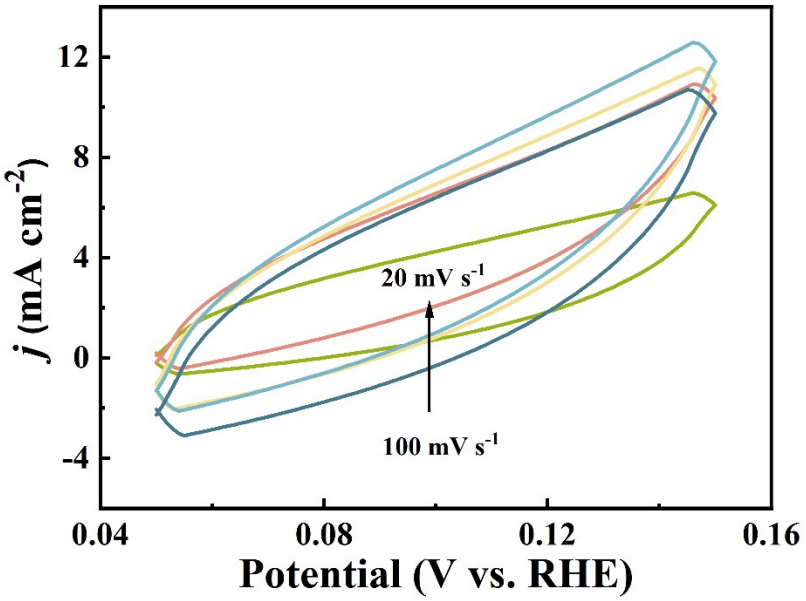

Figure S9 CV curves of Fe/Mn-$Ni_{0.85}Se$ after 100 h HER long-term stability test in the capacitance current range at various scan rates.

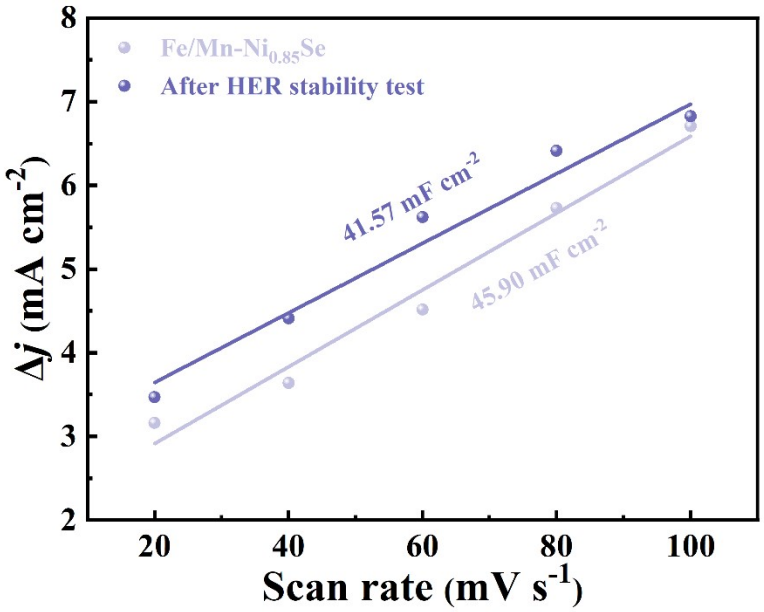

Figure S10 Capacitive current densities of Fe/Mn-$Ni_{0.85}Se$ after 100 h HER long-term stability test as a function of scan rate.

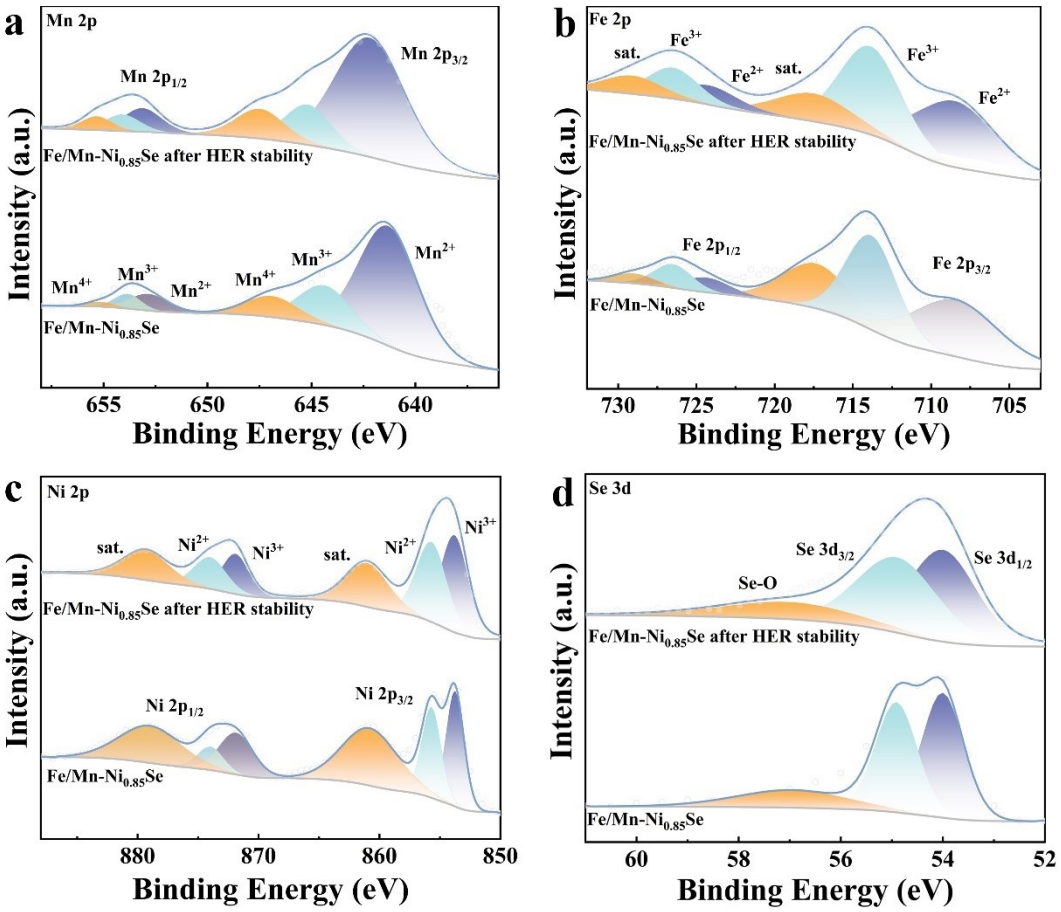

Figure S11 XPS spectra of (a) Mn 2p, (b) Fe 2p, (c) Ni 2p and (d) Se 3d for Fe/Mn-$Ni_{0.85}Se$ before and after HER stability tests.

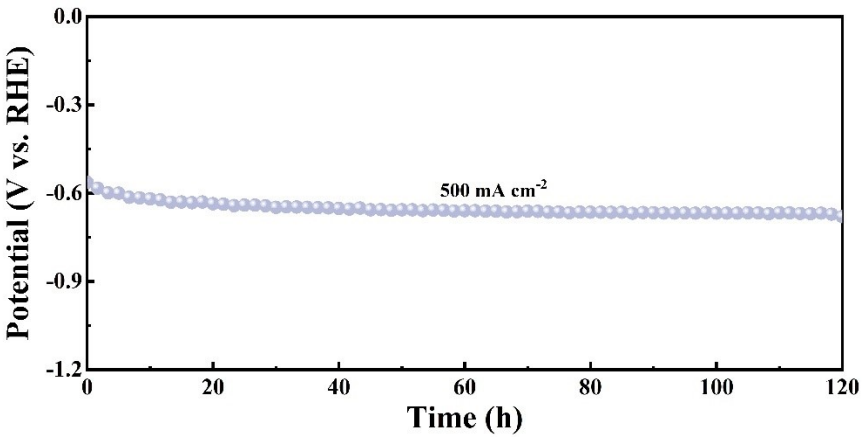

Figure S12 Chronopotentiometric curve of Fe/Mn-$Ni_{0.85}Se$ at 500 mA cm^{-2} for 120 h.

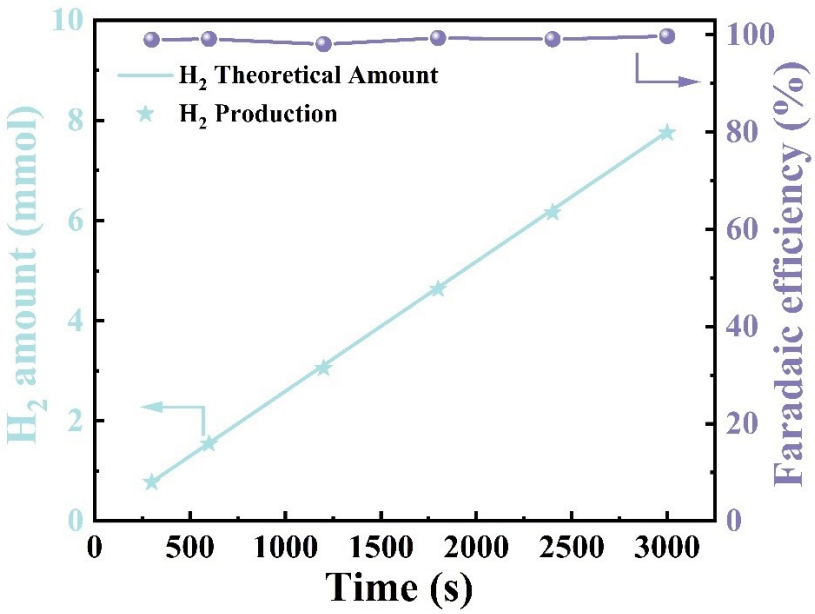

Figure S13 The evaluated H_2 amount and faradaic efficiency of Fe/Mn-$Ni_{0.85}Se$ for HER.

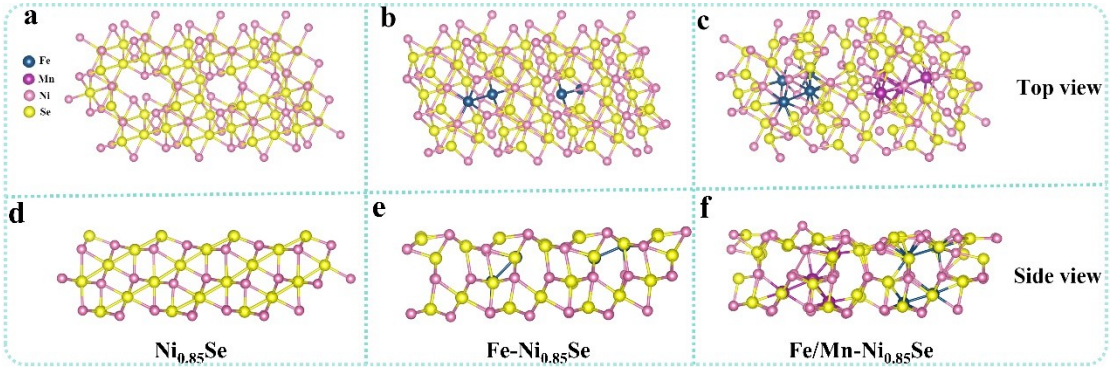

Figure S14 The side and top views of the optimized structures of (a,d) $Ni_{0.85}Se$, (b,e) Fe-$Ni_{0.85}Se$ and (c,f) Fe/Mn-$Ni_{0.85}Se$.

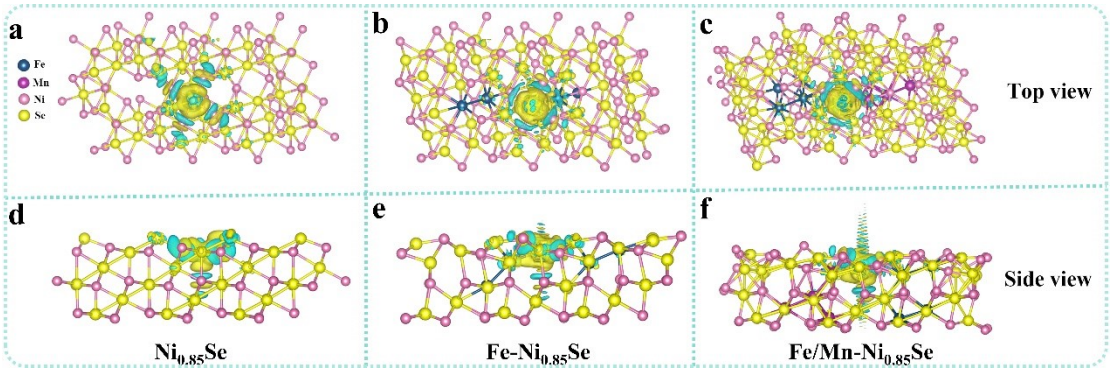

Figure S15 The charge density difference of $Ni_{0.85}Se$, Fe-$Ni_{0.85}Se$ and Fe/Mn-$Ni_{0.85}Se$.

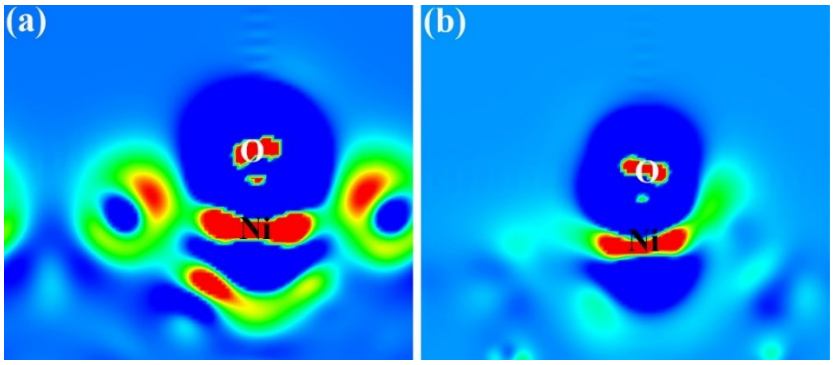

Figure S16 The charge density difference of $Ni_{0.85}Se$ and Fe-$Ni_{0.85}Se$ with adsorbed H_2O.

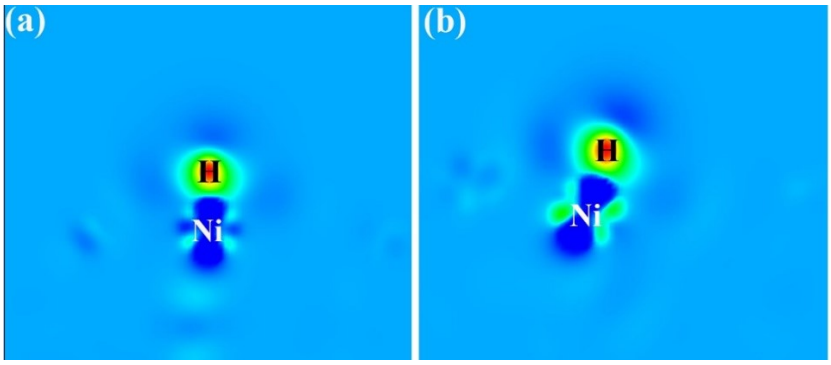

Figure S17 The charge density difference of $Ni_{0.85}Se$ and Fe-$Ni_{0.85}Se$ with adsorbed *H.

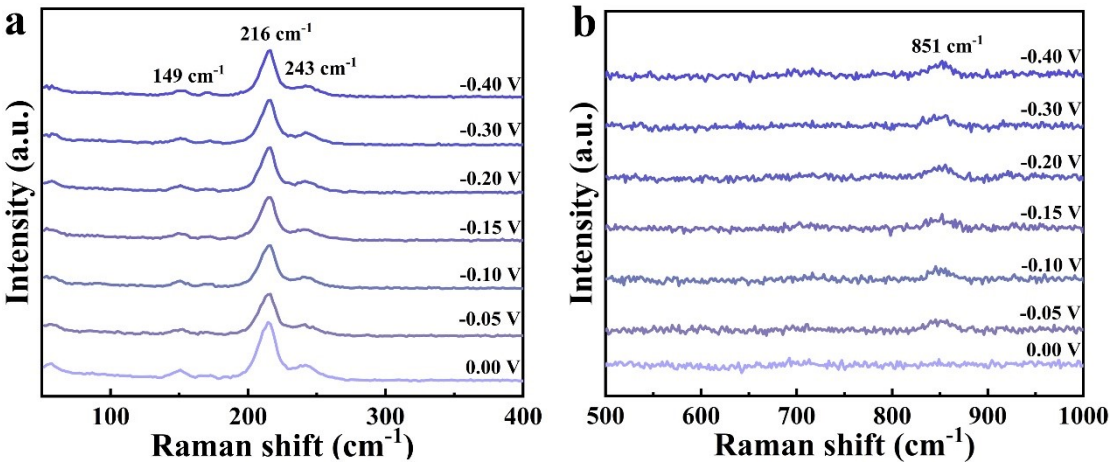

Figure S18 (a, b) In situ Raman spectra of Fe/Mn-$Ni_{0.85}Se$ with various applied potentials.

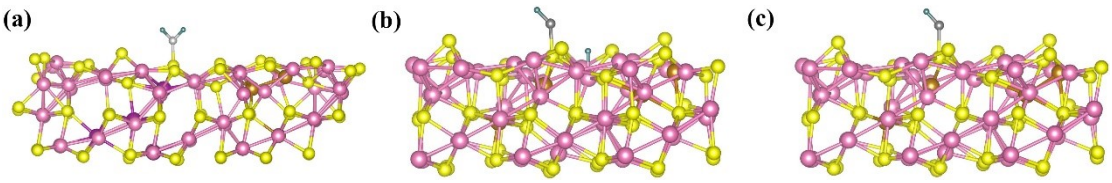

Figure S19 The optimized structures of adsorbed H_2O intermediates on $Ni_{0.85}Se$.

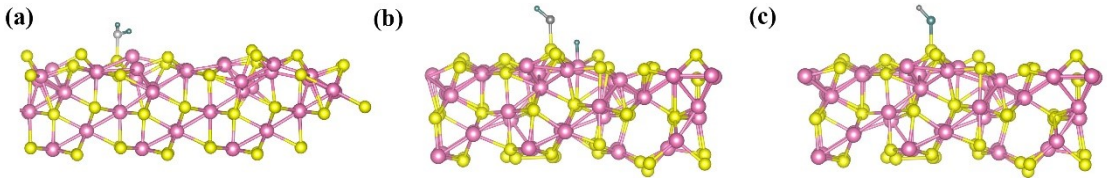

Figure S20 The optimized structures of adsorbed H_2O intermediates on Fe-$Ni_{0.85}Se$.

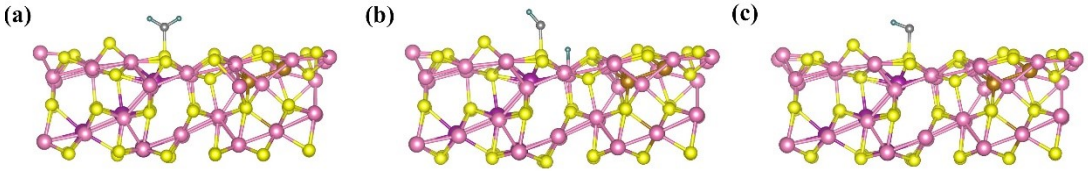

Figure S21 The optimized structures of adsorbed H_2O intermediates on Fe/Mn-$Ni_{0.85}Se$.

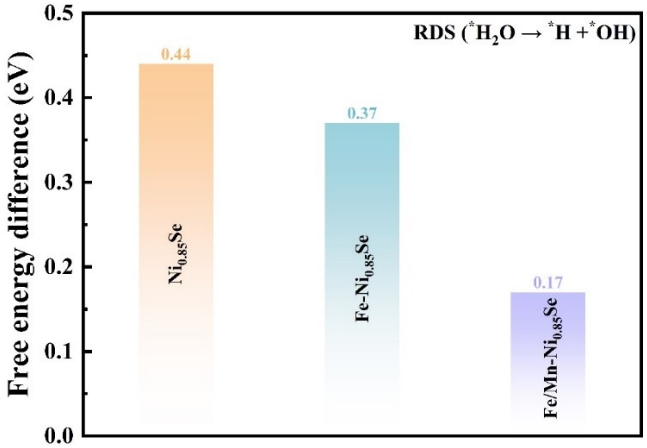

Figure S22 Free energy difference for RDS during water dissociation.

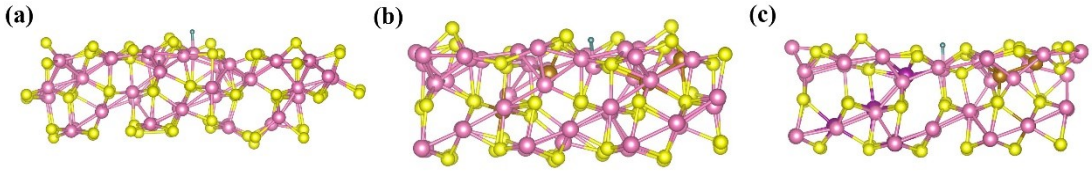

Figure S23 The optimized structures of adsorbed *H intermediate on (a) $Ni_{0.85}Se$, (b) Fe-$Ni_{0.85}Se$ and (c) Fe/Mn-$Ni_{0.85}Se$.

Table S1 Contents of Fe and Mn on the electrocatalysts by ICP-OES.

Electrocatalysts	Fe	Mn	Ratio of Fe/Mn
Fe-$Ni_{0.85}Se$	3.62%	--	--
Fe/Mn-$Ni_{0.85}Se$	3.72%	3.68%	1.01

Table S2 Summary information details of elements on $Ni_{0.85}Se$, Fe-$Ni_{0.85}Se$ and Fe/Mn-$Ni_{0.85}Se$ measured by XPS.

Samples	Element	Peak	BE (eV)	Relative area (%)
$Ni_{0.85}Se$	Ni 2p	Ni^{2+}	855.2/873.1	38.1
		Ni^{3+}	852.9/870.6	61.9
	Se 3d	M-Se	54.4/55.3	95.3
		SeO_x	57.5	4.7
Fe-$Ni_{0.85}Se$	Fe 2p	Fe^{2+}	708.1/724.1	21.8
		Fe^{3+}	713.2/726.3	78.2
	Ni 2p	Ni^{2+}	855.6/873.5	31.7
		Ni^{3+}	853.3/871.0	68.3
	Se 3d	M-Se	54.2/55.1	76.9
		SeO_x	57.3	23.1
Fe/Mn-$Ni_{0.85}Se$	Fe 2p	Fe^{2+}	708.3/724.3	45.9
		Fe^{3+}	713.5/726.6	54.1
	Mn 2p	Mn^{2+}	641.5/652.9	67.3
		Mn^{3+}	644.5/653.9	20.2
		Mn^{4+}	647.0/655.2	12.5
	Ni 2p	Ni^{2+}	856.1/874.0	46.6
		Ni^{3+}	853.8/871.5	53.4
	Se 3d	M-Se	54.0/54.9	88.2
		SeO_x	57.1	11.8

Table S3 A survey of the catalytic performance of various electrocatalysts for HER.

Electrocatalysts	Electrolyte	Electrocatalytic performance				Ref.
	KOH ($mol \cdot L^{-1}$)	j ($mA \cdot cm^{-2}$)	Overpotential (mV)	Tafel slope ($mV\ dec^{-1}$)	Stability	
$NiSe_2/Ni_3Se_4$/NF	1.0	10	142	72.9	60 h @ 10 mA cm^{-2}	[1]
NF/NiSe/Ni_3Se_2-Fe-5@5min	1.0	10	144	77	120 h @ 10 mA cm^{-2}	[2]
Fe-$NiSe_2$-Ni_3Se_4/NF-2	1.0	10	29	95.2	50 h @ 10 mA cm^{-2}	[3]
$Mo_{0.6}$-$CoSe_2$ NS@NF	1.0	10	89	69	10 h @ 10 mA cm^{-2}	[4]
$Mo_{0.2}$-Ni_3Se_2/NiSe	1.0	100	296	135	12 h @ 50 mA cm^{-2}	[5]
$NiFeSe_{0.6}$-MOF	1.0	10	156	193	72 h @ 5 mA cm^{-2}	[6]
V-$NiSe_2$/NF	1.0	10	100.7	74.2	30 h @ 20 mA cm^{-2}	[7]
P-$NiSe_2$	1.0	10 150	71 226	116	20 h @ 10 mA cm^{-2}	[8]
Fe-NiCoSe/NiCoSe/NF	1.0	10	120	132.6	150 h @ 10 mA cm^{-2}	[9]
Ni-Se-Yb/NF	1.0	10	50	60.4	72 h @ 50 mA cm^{-2}	[10]
Fe/Mn-$Ni_{0.85}$Se	**1.0**	**10** **500** **2000**	**22.4** **114.7** **136.4**	**37.0**	**120 h @ 500 mA cm^{-2}**	**This work**

References

[1] L. Tan, J. Yu, H. Wang, H. Gao, X. Liu, L. Wang, X. She and T. Zhan, *Appl. Catal. B: Environ*., 2022, **303**, 120915.

[2] R. Deng, H. Yao, Y. Wang, C. Wang, S. Zhang, S. Guo, Y. Li and S. Ma, *Chem. Eng. J*., 2024, **488**, 150996.

[3] H. Ding, X. Fan, X. Liu, L. Zhang and G.C. Xu, *J. Mater. Chem. A*, 2025, **13**, 16657-16670.

[4] J. Huang, S. Wang, J. Nie, C. Huang, X. Zhang, B. Wang, J. Tang, C. Du, Z. Liu and J. Chen, *Chem. Eng. J*., 2021, **417**, 128055.

[5] Y. Wu, H. Jin, X. Zhou, L. Guo and Q. Wang, *Int. J. Hydrogen Energy*, 2025, **145**, 644-652.

[6] Z. Luo, L. Tong, Z. Lin, R.S. Amin, J. Ren, K.M. El-Khatib and C. Wang, *Adv. Compos. Hybrid Mater.*, 2023, **6**, 159.

[7] M. Bai, T. Ai, W. Bao, J. Han, J. Zhang, Q. Yu, J. Liu, X. Wei, X. Zou and L. Feng, *J Mater. Sci. Tech*., 2024, **187**, 63-71.

[8] W. Yang, S. Wang, K. Zhao, Y. Hua, J. Qiao, W. Luo, L. Li, J. Hao and W. Shi, *J. Colloid Interface Sci*., 2021, **602**, 115-122.

[9] X. Fan, H. Ding, T. Huang, X. Liu, J. Xiao, M. Xie, G. Xu and L. Zhang, *ACS Appl. Nano Mater.*, 2024, **7**, 11530-11540

[10] S. He, L. Liu, Y. Yang, W. Liu, W. Tan and C. Zhou, *Fuel*, 2025, **382**, 133744.